PENETRATION DATA FOR A MEDIUM CALIBER TUNGSTEN SINTER ALLOY PENETRATOR INTO ALUMINUM ALLOY 7020 IN THE VELOCITY REGIME FROM 250 M/S TO 1900 M/S

Matthias Wickert

Fraunhofer Ernst-Mach-Institut, Eckerstr. 4, 79104 Freiburg, Germany
Phone: +49 761 2714-384 Fax: -1384 e-mail: matthias.wickert@emi.fraunhofer.de

Penetration data over a wide velocity range are of general interest for the ballistic research community. An important material class for light vehicle structures are aluminum alloys. Aluminum Alloy 7020 has been chosen to examine the semi-infinite penetration of a tungsten sinter alloy medium caliber type penetrator in the wide velocity regime from 250 m/s to 1900 m/s.

Three response regions are identified. Rigid body penetration is observed up to 700 m/s with the onset of plastic deformation of the penetrator's frustrum nose. A maximum depth of penetration of 1.4 of the penetrator's length is measured before the transition to hydrodynamic penetration with irregular shaped broad penetration craters sets in. Between 700 m/s and 1000 m/s a drastic drop up to 40% of the depth of penetration is observed due to strong bending of the penetration craters and the fragmentation of the penetrator. A penetration of 1.4 of the penetrator's length is exceeded again beyond impact

INTRODUCTION

High strength aluminum alloys are used for structural elements in infantry fighting vehicles. If such an element is considered as a target, the line-of-sight thickness might be drastically increased due to the target inclination relative to the shot line. Considering a target obliquity of 60° NATO and an azimuth angle of 45° NATO the resulting line-of-sight thickness is increased by a factor of 2.9. Since only few penetration data of tungsten sinter alloy penetrators in aluminum have been available so far, a test series was devoted to the penetration performance of a medium calibre type penetrator with a length over diameter ratio of 15 into the high strength Aluminum Alloy 7020 within the impact velocity regime from 250 m/s to 1900 m/s. All tests have been performed at the same gun facility employing single-stage powder gun setup and two-stage light-gas gun setup.

EXPERIMENTAL SETUP

The penetrator was shot with 0° NATO obliquity against the semi-infinite aluminum target represented by layering plates with a thickness of 60 mm and lateral dimensions of 125 mm x 125 mm. The high strength Aluminum Alloy 7020 with the composition AlZn4.5Mg1 is specified by the manufacturer with a minimum ultimate tensile strength of 350 N/mm², an elongation of 10% and a density of 2.77 g/cm³.

The tests were performed with a 90 mm long threaded penetrator with a frustrum nose, see figure 1. The nominal diameter is 6 mm. The mass of the penetrator is 46.7 g. The penetrator is made of a tungsten sinter alloy with a density of 17.7 g/cm³, an ultimate tensile strength of 1370 N/mm² and an elongation of 11.5%.

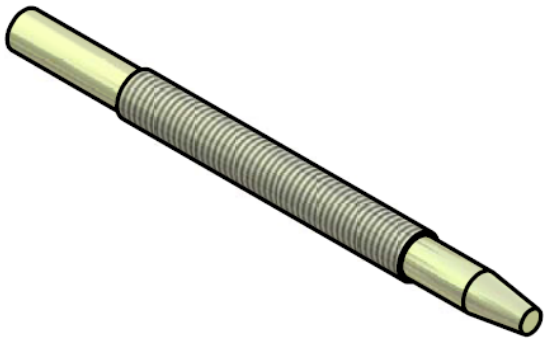

Figure 1 Frustrum nose tungsten sinter alloy penetrator.

RESULTS

Table 1 gives the penetration data measured in line-of-sight direction.

For high velocity the penetration in the aluminum alloy shall be compared to the penetration in RHA. In test 10759 the same penetrator was fired with a velocity of 1501 m/s and -0.1°/0° yaw against a semi-infinite RHA target with a hardness of BHN 300. The penetration of 71.5 mm in RHA compares to a value of 153 mm in Aluminum Alloy 7020 interpolated by the tests 10762 and 10763. Thus at 1500 m/s the tungsten sinter alloy penetrator exceeds in Aluminum Alloy 7020 the penetration in RHA by a factor of 2.1. For comparison images of the penetration craters of test 10759 and 10762 are shown in figure 2. Images of the penetration craters for almost all aluminum targets are displayed in figure 3.

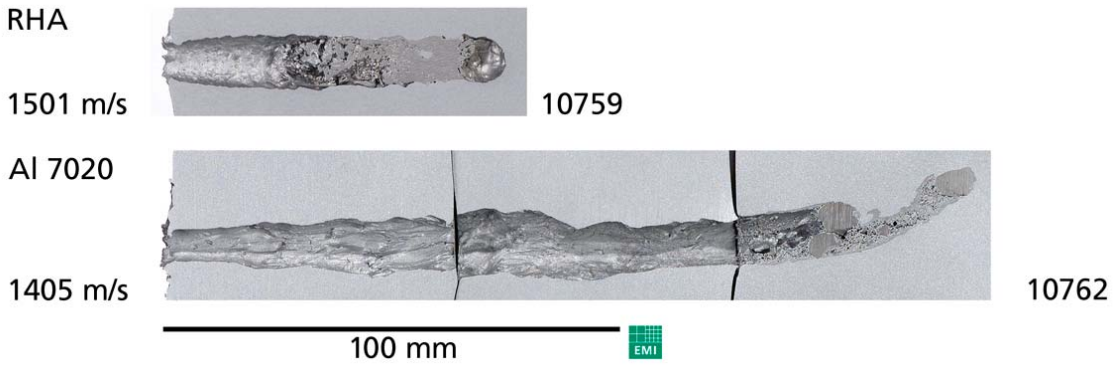

Figure 2 Comparison of penetration craters into RHA (10759) and Aluminum Alloy 7020 (10762) at high striking velocity.

Table 1 Semi-infinite penetration data for Aluminum Alloy 7020.

Velocity [m/s]	Test ID	Pitch/Yaw [°]	Penetration [mm]	Penetration [P/L]
221	10809	-0.1/0.3	16.2	0.18
251	10810	-1.3/1.1	28.6	0.32
335	10803	0.9/-1.1	43.5	0.48
461	10806	0.1/0.2	77.4	0.86
540	10798	0/-0.1	102.5	1.14
664	10804	0.1/-0.1	112.6	1.25
695	10808	0.5/-0.3	122.3	1.36
785	10805	0.3/-0.5	71.6	0.80
869	10797	-0.3/0	78.3	0.87
884	10812	-/-	80.9	0.90
946	10807	0.1/-0.1	111.8	1.24
1071	10799	-0.5/0.7	127.2	1.41
1264	10800	0.2/0.2	142.5	1.58
1405	10762	-0.3/-0.2	172.2	1.91
1670	10763	-0.6/-0.4	190.2	2.11
1924	10813	0.6/-0.2	225.4	2.50

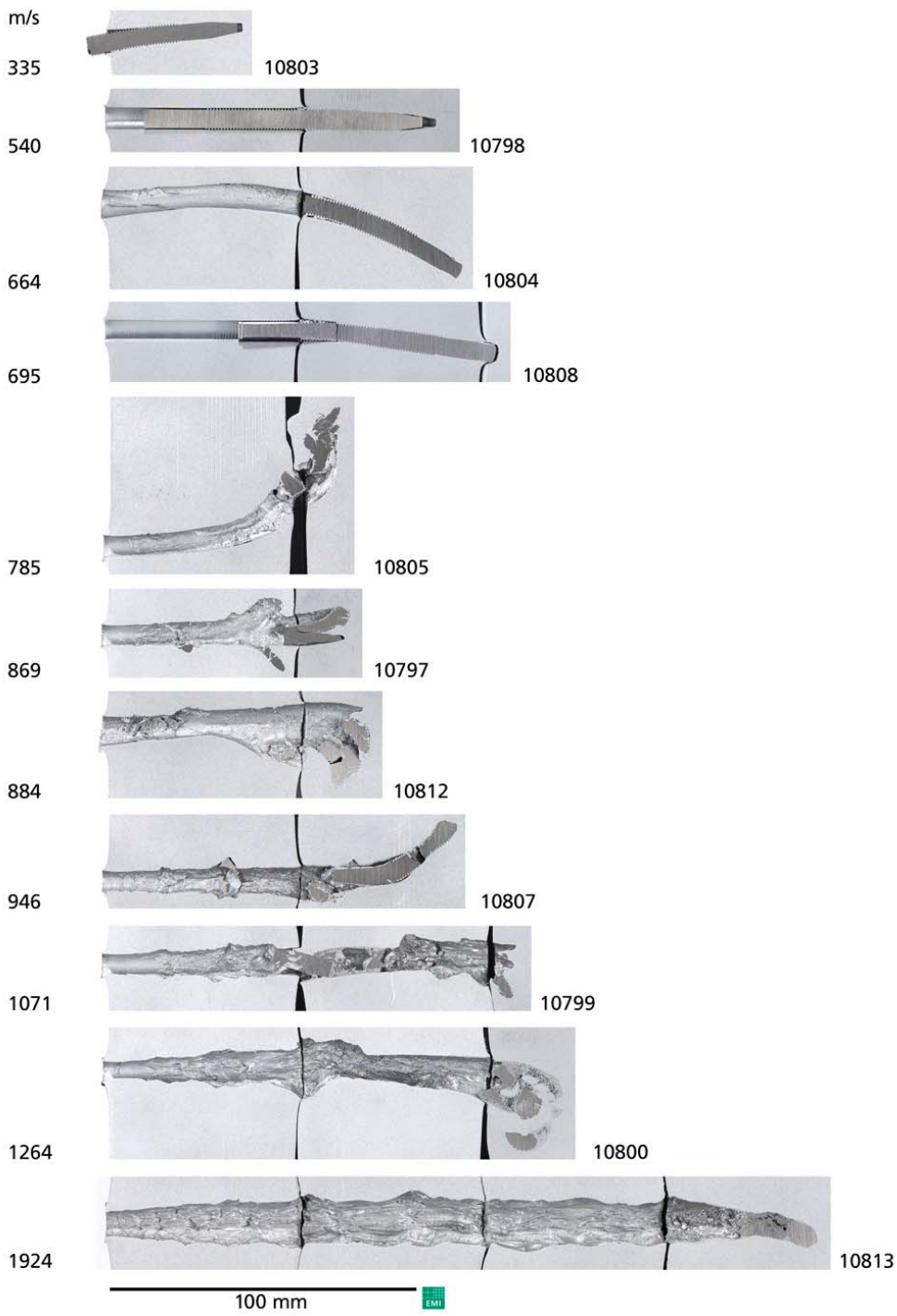

Figure 3 Penetration craters in Aluminum Alloy 7020 with respect to impact velocity.

Comparing the cross-sectional shapes of the projectile nose, the onset of projectile deformation can be observed at 664 m/s in test 10804. In figure 3 the nose shape is compared for this and the nearby-velocity tests. At 540 m/s in test 10798 the frustrum nose shape is still intact whereas at 695 m/s in test 10808 the nose shape has deformed to a flat shape.

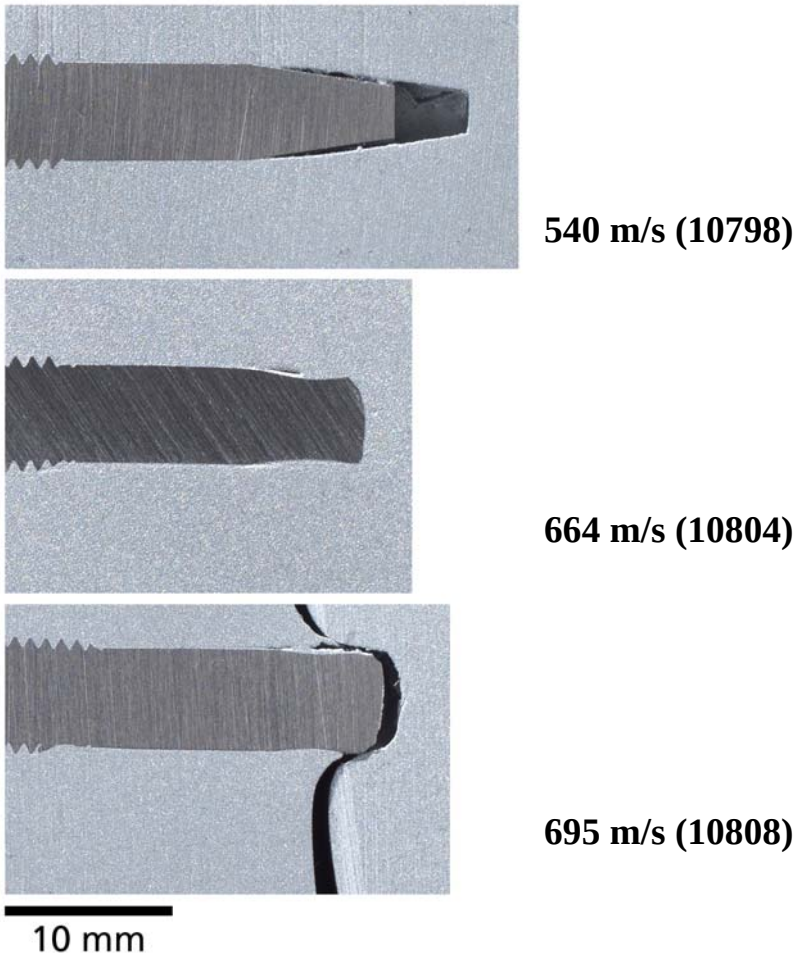

Figure 3 Onset of frustrum projectile nose deformation.

The penetration data are graphically presented in figure 4 with three response regions. Up to 700 m/s a parabolic fit function is inserted based on the penetration data up to 540 m/s without plastic deformation of the penetrator nose, reflecting that the amount of displaced target material is proportional to the kinetic energy of the projectile.

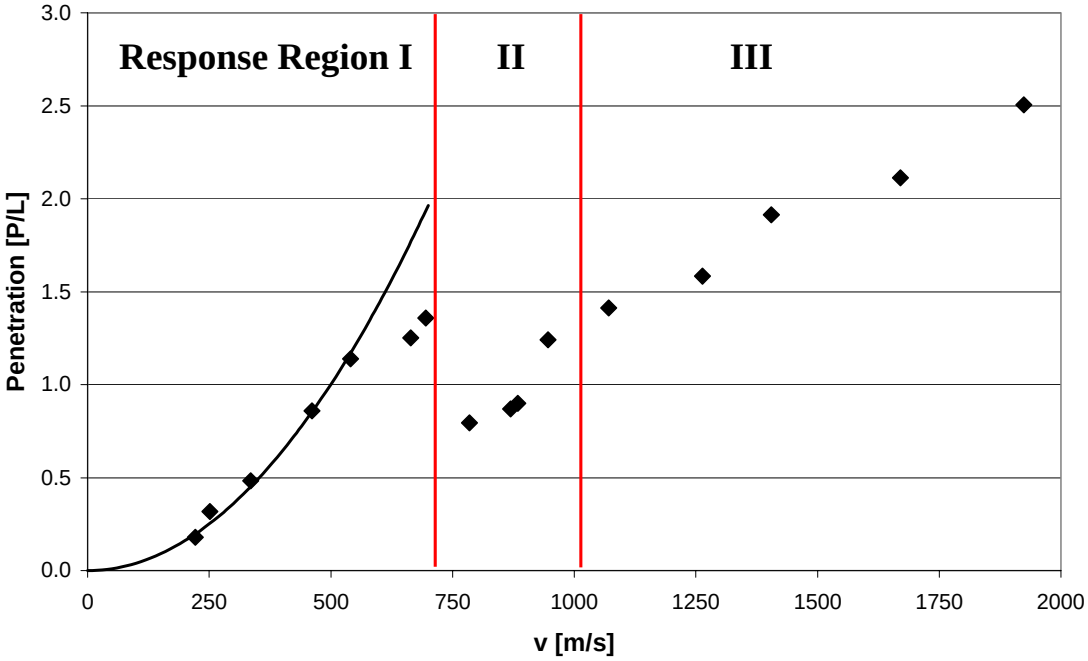

Figure 4 Drop of semi-infinite penetration into Aluminum Alloy 7020 at 700 m/s.

A steep increase in penetration up to 1.4 penetrator lengths is observed up to a velocity of 700 m/s with penetration craters that are straight or modestly bent. The penetrator is visible to a large extent in the target cross section images and fits tightly in the smooth crater channels. For the following three tests at velocities of 785 m/s, 869 m/s and 884 m/s drastically reduced penetration values are observed – about 40% less than the penetration measured at 695 m/s. At 946 m/s the depth of penetration is still 9% less than at the test at 695 m/s. There is no indication that this reduction of penetration performance is related to an increased yaw in the corresponding velocity regime. But the penetration craters are either strongly bowed as in test 10805 or crater branching does occur as in test 10797. In all of these tests the penetrator is strongly fragmented and the penetration channels are at least in some sections much wider than the penetrator diameter.

Not until 1071 m/s the penetration performance exceeds the value at 695 m/s. This corresponds to a velocity increase of almost 400 m/s or, respectively, an increase of the kinetic energy of the penetrator by a factor of 2.4. Beyond velocities of 1000 m/s the penetration craters are to a large portion directed along the line-of-sight axis with modest bowing at the end. The walls of the crater walls are irregular and the penetrator is fragmented and eroded.

DISCUSSION

Tungsten sinter alloy penetrators are often designed for high performance in steel targets. For high impact velocities pure hydrodynamic theory estimates the ratio P/L for a tungsten sinter alloy penetrator with the density ρ_p=17.7 g/cm³ and steel with the density ρ_{st}=7.85 g/cm³ according to eq.(1) to 1.5.

$$\frac{P}{L} = \sqrt{\frac{\rho_P}{\rho_t}} \tag{1}$$

For an aluminum target with ρ_{al}=2.77 g/cm³ the estimate is 2.5. For long rod penetration in steel, this estimate by pure hydrodynamic theory describes the magnitude of penetration values achieved for high velocities beyond 2500 m/s reasonably well, whereas for the penetration in aluminum a magnitude of 3.5 is reported [1] attributed to a strong contribution of secondary penetration effects.

Tate's [2] modified hydrodynamic theory takes strength effects into account and estimates the necessary velocity v_{thres} for a penetrator beginning to deform by eq. (2).

$$v_{thres} = \sqrt{2\frac{Y_p - R_t}{\rho_t}} \tag{2}$$

Below this velocity rigid body penetration will occur. By approximating the dynamic strength of the projectile Y_p and the target R_t by the tensile strength data given before, the threshold velocity for the RHA target is about 290 m/s whereas the limit velocity for the Aluminum Alloy 7020 is estimated by 860 m/s. Due to the much higher threshold velocity, rigid body penetration effects become much more visible in aluminum targets compared to steel targets.

The data presented for the aluminum penetration by a tungsten sinter alloy penetrator reflect this transition from rigid body penetration to hydrodynamic penetration with rod erosion and mass consumption. For the tungsten sinter alloy penetrator used in the experiments, rigid body penetration yields very high penetration values up to a velocity of 700 m/s. Then the penetration performance drops more than 40 % and beyond velocities of 1000 m/s the penetration performance exceeds the maximum depth for rigid body penetration again.

Maximum rigid body penetration and the transition velocity depend strongly on the shape and hardness of the projectile nose. Forrestal and Piekutowski [3] have demonstrated for the penetration of a steel projectile into Aluminum 6061-T6511, that for an ogival nose shape rigid body penetration can be observed up to velocities as high as 1400 m/s with a resulting penetration of about 4 P/L whereas for a spherical nose

rigid body penetration was observed only up to a velocity of 1000 m/s with 1.3 P/L. Also the positive effect of high projectile hardness on the maximum rigid body penetration performance is demonstrated there.

For the tungsten sinter alloy penetrator in the response region of rigid body penetration into the Aluminum Alloy 7020 the penetration data can well be fitted by a parabolic curve. The onset of projectile nose deformation in tests 10804 and 10808 is correlated with reduced penetration relative to the parabolic fit curve.

The specific characteristics of the penetration behaviour for the transition from rigid body penetration to hydrodynamic penetration will depend strongly on nose form and strength of the penetrator.

CONCLUSIONS

For the tungsten sinter alloy penetrator with frustum nose design rigid body penetration into the Aluminum Alloy 7020 was observed up to 700 m/s with a maximum penetration of 1.4 P/L. In the transition region the penetration performance for the examined penetrator design drops by 40% before the same penetration performance is reached again at velocities beyond 1000 m/s and rises to 2 P/L at 1500 m/s.

The onset of the plastic deformation of the frustrum penetrator nose was observed at 661 m/s with reduced penetration relative to a parabolic fit curve for rigid body penetration.

Penetrator erosion and mass consumption become important for velocities greater than 1000 m/s with irregular crater walls and a modest bowing at the end of the penetration crater. At a velocity of 1924 m/s the hydrodynamic penetration limit is closely reached with minor secondary penetration effects due to rigid body penetration in the final penetration phase.

REFERENCES

[1] A. J. Stilp, V. Hohler, Long rod penetration mechanics, Chapter No. 5 in *High velocity impact dynamics*, Editor J. A. Zukas, John Wiley & Sons, New York (1990)
[2] A. Tate, Further results in the theory of long rod penetration, *J. Mech. Solids*, Vol. 17, 141-150 (1969)
[3] M. J. Forrestal, A. J. Piekutowski, Penetration experiments with 6061-T6511 aluminum targets and spherical-nose steel projectiles at striking velocities between 0.5 and 3 km/s,
International Journal of Impact Engineering 24, 57-67 (2000)